PAPER

Multifunctionality of structural nanohybrids: the crucial role of carbon nanotube covalent and non-covalent functionalization in enabling high thermal, mechanical and self-healing performance

To cite this article: Marialuigia Raimondo *et al* 2020 *Nanotechnology* **31** 225708

IOP Publishing Nanotechnology
Nanotechnology 31 (2020) 225708 (16pp) https://doi.org/10.1088/1361-6528/ab7678

Multifunctionality of structural nanohybrids: the crucial role of carbon nanotube covalent and non-covalent functionalization in enabling high thermal, mechanical and self-healing performance

Marialuigia Raimondo[1,5], Carlo Naddeo[1], Luigi Vertuccio[1], Leila Bonnaud[2], Philippe Dubois[2], Wolfgang H Binder[3], Andrea Sorrentino[4] and Liberata Guadagno[1,5]

[1] Department of Industrial Engineering, University of Salerno, Via Giovanni Paolo II, 132, I-84084, Fisciano (SA), Italy
[2] Laboratory of Polymeric and Composite Materials, Center of Innovation and Research in Materials & Polymers (CIRMAP), Materia Nova Research Center & University of Mons, 20 Place du Parc, B-7000-Mons, Belgium
[3] Macromolecular Chemistry, Institute of Chemistry, Faculty of Natural Science II, Martin Luther University Halle-Wittenberg, Von-Danckelmann-Platz 4, D-06120, Halle (Saale), Germany
[4] Institute for Polymers, Composites and Biomaterials (IPCB-CNR), via Previati n. 1/E, I-23900, Lecco, Italy

E-mail: mraimondo@unisa.it and lguadagno@unisa.it

Received 17 October 2019, revised 7 January 2020
Accepted for publication 14 February 2020
Published 13 March 2020

Abstract

This study proposes new kinds of functionalization procedures able to preserve specific properties of carbon nanotubes (CNTs) and to improve compatibility with the epoxy matrix. Through a covalent approach, for the first time, CNTs are functionalized with the same hardener agent, 4,4′-diaminodiphenyl sulfone, employed to solidify the epoxy matrix and capable to fulfill mechanical requirements of industrial structural resins. The same CNTs are non-covalently modified through the polymer wrapping mechanism with benzoxazine (Bz) terminated polydimethylsiloxane (PDMS). The comparison between electrical and mechanical properties of the nanocomposites highlights the success of the non-covalent functionalization in determining an increase in the glass transition temperature (Tg) and in better preserving the unfunctionalized CNT electrical conductivity. Besides, tunneling atomic force microscopy (TUNA), powerful to catch ultra-low currents, has been used for revealing the morphology on nanoscale domains and detecting the conductivity on the same location of CNT/epoxy resins. No electrical contacts to the grounds have been used for the TUNA analysis; a procedure that does not alter the results on the interface domains which experience contact areas with strong differences in their properties. The effectiveness of performed CNT functionalizations as a route to impart self-healing efficiency to the resin formulations has also been proved.

[5] Authors to whom any correspondence should be addressed.

Supplementary material for this article is available online

Keywords: carbon-based composites, smart materials, surface properties, interface/interphase, covalent and non-covalent functionalization of carbon nanotubes, tunneling atomic force microscopy (TUNA)

(Some figures may appear in colour only in the online journal)

1. Introduction

Since their discovery in 1991 [1], carbon nanotubes (CNTs) have captured increased attention because of their unique combination of exceptional thermal, electrical and mechanical properties [2–7]. CNTs represent an ideal reinforcing agent for fabricating high strength epoxy structural composites with improved functional properties [8–13]. In this regard, many research attempts have been directed towards producing CNT/polymer composites for several applications [14–18]. However, the severe drawbacks associated with dispersion of entangled CNTs during processing together with poor interfacial interactions between CNTs and polymer matrix [19] greatly hinder their use as reinforcement [3, 20–22]. CNT surface functionalization [23–25] is an effective way to overcome these drawbacks. In fact, it does not only gives rise strong interfacial interactions improving the load transfer across the CNT-polymer matrix interface [26] but also induces better compatibility between CNTs and the polymer matrix [10]. CNT surface can be modified with several functional groups through two different strategies, such as a covalent approach (based on the covalent chemical functionalization) or a non-covalent approach (based on the physical interactions between matrix molecules and functional groups or molecular functional structures on the CNTs). Covalent functionalization, in turn, could also be divided into direct covalent sidewall functionalization and indirect covalent functionalization with carboxylic groups on the CNT surface. There are advantages and disadvantages to both approaches. The main advantage of the covalent functionalization is the high dispersion stability while providing useful functional groups on the CNT surface. The covalent methods, in turn, can induce a large number of defects on the CNT sidewalls and, in the worst cases, they can also lead to the breaking of CNTs into fragments with a loss of inherent properties. Furthermore, direct covalent sidewall functionalization is associated with a change of carbon atoms hybridization from sp^2 to sp^3 and a simultaneous loss of π-conjugation related to the graphene layers. The non-covalent functionalization is an alternative method for tuning the interfacial properties of CNTs. It can be achieved through π–π interaction and/or polymer wrapping process through both van der Waals type's interactions and π–π stacking between CNTs and polymer chains bringing along aromatic rings. The non-covalent functionalization of CNTs with molecules showing a strong affinity with CNT graphitic surfaces is a very hopeful strategy to modify the CNT surface without compromising their structural integrity [11, 27, 28]. It preserves the inherent properties of CNTs with supramolecular interactions and introduces an additional interface between nanofiller and matrix. The main advantages of the non-covalent functionalizations are the easy and universality of the preparation procedure and the absence or reduction of the nanofiller damage, thus providing an effective solution for preserving its functional and structural properties [3, 11, 27–29]. The inherent disadvantage is represented by weak interaction stability [29–31]. More in-depth investigations are necessary to obtain better tailoring of the functional groups responsible for balancing the intensity of the interactions with the mechanical forces that determine the weakening of the interactions [30–34]. The most promising and effective method is therefore based on the achievement of naturally strong interactions between the CNTs and the matrix. Various inorganic and organic functional molecules can involve adsorption onto the CNT sidewall via π–π stacking, van der Waals or charge transfer interactions. Among them, π–π stacking is the strongest interaction of delocalized π-bonds between CNT walls and functional molecules [11, 35]. A typical approach is the non-covalent bonding of CNTs with polymers containing pendent pyrene groups. Pyrene derivatives are ideal molecules for π–π interactions with CNTs since their aromatic system is analogous to graphite. In our recently published work [11], we have proved that by modifying non-covalently the multi-wall CNTs (MWCNTs) via π-stacking interaction between MWCNTs and a pyrene derivative, the electrical properties have been preserved. In fact, this type of functionalization has allowed us to obtain values of electrical percolation threshold (EPT) similar to those obtained for nanocomposites loaded with unfunctionalized MWCNTs, i.e. lower than 0.28%. but with an increase in electrical conductivity above the EPT [11]. Starting from these promising results [11], this work represents a successful attempt to obtain nanohybrids with high thermal and mechanical performance, which are potentially able to satisfy the impelling needs established by the aeronautical industries, safeguarding the electrical conductivity. Both the covalent and non-covalent (via the polymer wrapping mechanism) approaches have been followed. In this work, unfunctionalized CNT, covalently functionalized CNT with DDS ligand (CNT–DDS) and CNT modified through a non-covalent approach (via the polymer wrapping mechanism) with benzoxazine (Bz) terminated polydimethylsiloxane (PDMS) (CNT–PDMS–Bz) were dispersed within an epoxy matrix. Polymer wrapping through non-covalent interactions (comprising $\pi-\pi$, CH$-\pi$, and cation$-\pi$) which act by adsorbing on the CNT surface is a kind of dispersion, appealing as regards the stability and homogeneity of the functionalization [36]. DDS ligand and PDMS–Bz modifier have proved to be

effective in improving the dispersion while preserving the electrical conductivity of the epoxy samples, which is comparable to the resins filled with pristine CNT. It is known that carbon nanofiller can interrupt the network density in the nanodomains at the interface between CNT walls and matrix [8]. DDS ligand may play a meaningful role as an additional hardening agent for epoxy curing systems at the interface nanofiller/matrix. Furthermore, recently, enormous attention has been paid to the addition of CNTs in polybenzoxazines in order to improve the performance of the corresponding nanocomposites [37–45]. It has been found that it is possible to obtain a hardened network characterized by extraordinary thermo-mechanical properties as a consequence of the inherent interactions between the CNTs and a benzoxazine resin [33, 40, 41]. The polydimethylsiloxane (PDMS) polymer used in combination with benzoxazine (Bz) resin to form polydimethylsiloxane-benzoxazine prepolymer (PDMS–Bz) allows improving the mechanical and thermal properties of the final epoxy nanocomposites. It has been found that the use of PDMS, as mechanical reinforcement, is extremely sought after and necessary to develop lightweight and flexible materials in matter-of-fact employments. In fact, PDMS polymer is a renowned elastomer with multifaceted and charming properties such as superb chemical stability, high thermal resistance, limited toxicity, very low glass transition temperature (Tg), unequaled linear elasticity over an extended range of temperatures ranging from −40 °C to 400 °C and strains. For these reasons, it is used in numerous sectors, namely automotive, aerospace, building, and electric [46].

The focus of this paper is the functionalization of CNTs by applying these interesting described different approaches like covalent bonding (CNT–DDS) and physical adsorption (CNT–PDMS–Bz). These kinds of functionalizations have been selected to fulfill one or more of the following requirements: (a) to enable efficient dispersion of nanofillers during nanocomposite preparation; (b) to confer/preserve specific functions and/or properties such as suitable electric conductivity, high thermal stability and auto-repair function. Although the covalent approach is well studied in literature, the covalent functionalization with DDS ligand is a completely new approach and poses many questions. In fact, for this kind of functionalization, the very important issue was to study if the $-NH_2$ of the DDS were able to activate cross-linking reactions or not (due to the reduced mobility and the steric effects). In the second case, the preservation of NH_2 groups would have enabled reversible self-healing interactions via hydrogen bonds. All prepared functionalized CNTs and related nanocomposites have been extensively characterized via thermogravimetric analysis (TGA), Fourier transform infrared spectroscopy (FTIR), Raman measurements as well as dynamic mechanical analysis (DMA) and TUNA, which has been performed for the its potentiality to allow a comparison between morphology and electrical properties at nanometric level of the functionalized and unfunctionalized CNTs/resins [47, 48]. The choice to modify the surface of the CNTs both through these particular covalent and non-covalent approaches has proved to be advantageous for obtaining homogeneous dispersion of the functionalized fillers inside the resin, due to the enhancement of the interface interaction between polymer and filler, and for increasing the thermo-oxidative stability of nanocomposites. The chosen functionalizations have proven to be effective strategies to confer self-healing ability to the nanocomposites. In particular, the non-covalent functionalization, maintaining the inherent CNT properties with various supramolecular interactions, allows obtaining the highest healing efficiency value, up to 350% with respect to all nanofilled samples investigated in this paper. The reference sample containing unfunctionalized CNTs shows no healing efficiency, so highlighting the effectiveness of functionalization also in imparting self-repairing functionality to the epoxy mixture.

2. Experimental

2.1. Materials

MWCNTs (Nanocyl S.A.-3100 Grade), here named CNT, were used. The uncharged sample was obtained by mixing the tetraglycidyl methylene dianiline (TGMDA) with a reactive diluent 1,4-butanediol diglycidyl ether (BDE), capable to decrease the moisture content and viscosity of the material, thus facilitating the dispersion step of nanofiller [8, 9, 11, 47–52], ameliorating the workability and easiness of processing and thus optimizing performance properties. The 4,4′-diaminodiphenyl sulfone (DDS) was used as hardening agent. TGMDA, BDE, and DDS were obtained from Sigma-Aldrich.

2.2. Covalent and non-covalent functionalization of CNTs

The CNT surface was modified following both covalent and non-covalent approaches. The covalent interaction occurred through the synthesis of unfunctionalized CNT modified with DDS ligand in a diazonium reaction, leading to the covalently functionalized CNT–DDS (see the synthesis scheme of figure 1(a)).

The CNT surface was modified following both covalent and non-covalent approaches (see scheme of figure 1(a)). The covalent interaction occurred through the synthesis of unfunctionalized CNT modified with DDS ligand. This functionalization procedure is based on the diazonium reaction through the diazotization reaction, which produces the diazonium salt (made *in situ* to contrast the instability). In this synthesis procedure, the DDS hardener was used as the primary arylamine for the *in situ* generation of the diazonium salt. The reaction was kept overnight. The product was vacuum filtered and washed with DMF until the liquid filtrate was colorless.

DDS modified carbon nanotubes (CNT–DDS) are able to play an important role as an additional hardening agent for epoxy curing systems enabling a much better dispersion compared to pristine CNT and also guaranteeing good electrical, mechanical and thermal performance of the nanocomposite material. The covalent functionalization procedure is based on the diazonium reaction, wherein DDS was used as the primary arylamine for the *in situ* generation of the

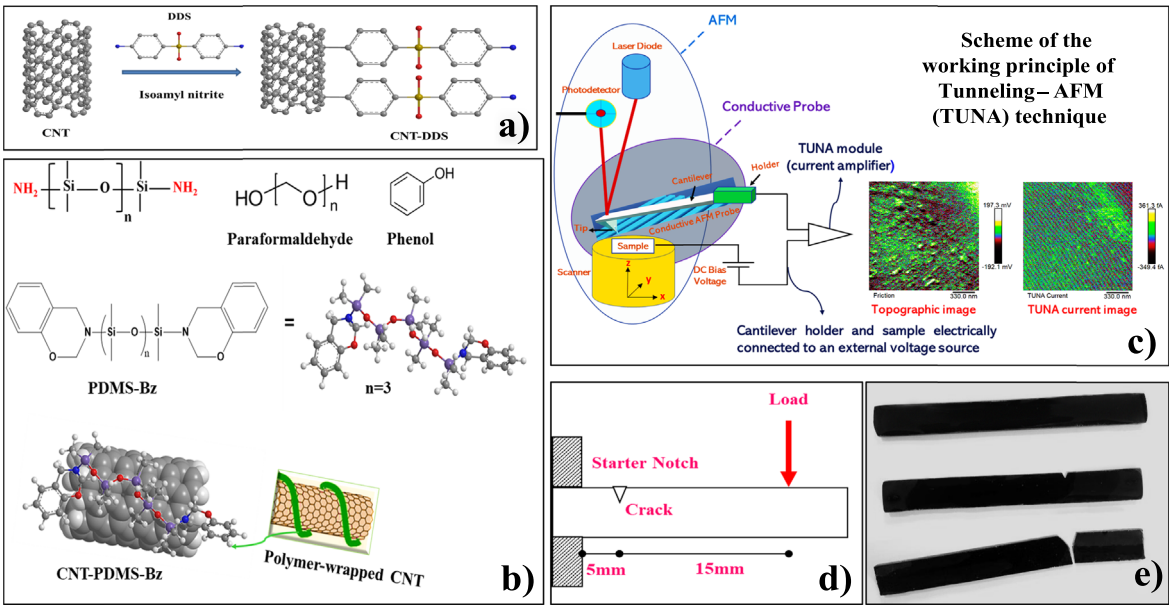

Figure 1. (a) Synthesis scheme of DDS functionalized carbon nanotubes (CNT–DDS), (b) chemical formulas of the molecules aimed at the preparation of carbon nanotubes modified with PDMS–Bz (CNT–PDMS–Bz), (c) schematic of tunneling AFM (TUNA) technique, (d) test geometry adjusted for the healing experiments and (e) epoxy samples before and after healing tests.

diazonium salt. For this purpose, pristine CNT and DDS were dispensed under inert conditions. Subsequently, isoamyl nitrite was added and the mixture was stirred overnight. The synthesized CNT–DDS was filtered and washed with DMF until the liquid filtrate was colorless. Finally, the obtained product was dried in a vacuum oven. The filtration step was the most challenging step due to the larger amount of CNTs. In this regard, it is good to specify that also and especially in a possible up-scaling process, the filtration turns out to be the limiting process regarding the preparation of larger amounts. Nevertheless, we were able to prepare 3 g of CNT–DDS nanofiller.

Non-covalent functionalization can be achieved through the π–π interactions of CNTs with electron-rich molecules. The non-covalent interactions of CNTs with small molecules other than π–π interactions lead to adsorption. Adsorption could also originate from molecular interactions between carbon-hydrogen groups (CH groups) and π systems and the existence of CH–π interactions has been known for several years [53]. Silicone is incorporated within the epoxy matrix by taking advantage of polydimethylsiloxane (PDMS) high affinity towards CNTs. Indeed, PDMS chains possess a strong ability to adsorb onto the CNTs and wrap around them through CH–π interactions between the PDMS methyl groups and the π-electron-rich surface of CNTs [54]. Nevertheless, PDMS is also known to be highly incompatible with epoxy matrices leading to a macro-phase separation between these two components. To overcome this drawback and to promote epoxy/PDMS compatibilization, PDMS chains bearing terminal reactive functions towards the epoxy system were thus considered. The non-covalent approach took place through the incorporation and dispersion of CNTs into the benzoxazine terminated polydimethylsiloxane (PDMS–Bz). It is worth noting that benzoxazines belong to a new class of thermosetting resins, which are often used as high-performance matrices for composites. More specifically, they consist of heterocyclic monomers, which can be easily synthesized either in bulk or in a solvent with a yield of reaction higher than 90% from the phenols, amines, and formaldehyde. Due to the relative abundance of these compounds, benzoxazine precursors exhibit a great versatility of design with the possibility to consider the incorporation of additional functionalities in their structure. Benzoxazine resins are found to be easily cured without the need of hardeners or catalysts and they can exhibit high glass transition temperature after curing. In recent times, benzoxazine resins have aroused widespread interest due to their ability to bring together the exceptional properties of traditional epoxy and phenolic resins. In particular, they are found to exhibit high thermal stability and form important char yield upon thermal degradation. Besides, the benzoxazine resins are compatible and reactive towards epoxy resins. Thus, the CNT dispersion could be obtained readily and did not need additional functionalization because of an extraordinary intrinsic affinity with the precursor. More precisely, the preparation of CNT–PDMS–Bz was carried out according to the procedure that can be summarized as follow. Firstly, PDMS–Bz was synthesized and, in this regard, the synthesis was performed in bulk from amino-terminated PDMS (800 g mol^{-1} from ABCR), paraformaldehyde and phenol (purchased from Sigma-Aldrich) in a stoichiometric ratio of 1:4.4:2 at 120 °C for 20 min. Subsequently, the CNTs were impregnated with 800 g mol^{-1} PDMS–Bz via the preparation of high loaded masterbatches (MB) with CNT/PDMS ratio kept constant to 50wt%:50wt%, giving the non-covalently functionalized nanofillers CNT–PDMS–Bz. Figure 1(b) shows the chemical formulas of the compounds used for the preparation of CNT–PDMS–Bz.

2.3. Preparation of epoxy samples

TGMDA (T) and BDE (B) were mixed at 80% and 20% by weight, respectively, providing the sample TB. Afterwards, the DDS (D) was completely solubilized in a stoichiometric quantity in the TB mixture, thus leading to the uncharged formulation TBD. Finally, the nanocomposites TBD+1% CNT, TBD+1%CNT–DDS, TBD+1%CNT–PDMS–Bz and TBD+0.5%CNT–PDMS–Bz were obtained by dispersing in TB epoxy matrix (with an ultrasonicator for 20 min) the unfunctionalized CNT and functionalized CNT–DDS and CNT–PDMS–Bz at loading concentration of 1 wt%, also using the additional percentage of 0.5 wt% of CNT–PDMS–Bz, before adding the DDS. These load level percentages of functionalized CNT–DDS and CNT–PDMS–Bz were chosen for comparison with pristine CNT since, for these nanofiller quantities, the electrical conductivity values shown by the CNT-based nanocomposites were beyond the EPT [8, 11, 49]. Furthermore, these formulations also showed good dynamic-mechanical properties [8, 9, 49]. All the samples were cured in two isothermal stages of which the first was carried out at 125 °C for 1 h and the second at 200 °C for 3 h [8, 9, 11, 47–49].

2.4. Characterization

In this work, we have carried out the following characterizations: DMA, FTIR spectroscopy, differential scanning calorimetry (DSC), TGA, field emission scanning electron microscopy (FESEM), high-resolution transmission electron microscopy (HRTEM), electrical measurements of direct current (DC) conductivity, tunneling atomic force microscopy (TUNA), RAMAN spectroscopy, self-healing efficiency. Experimental details related to the aforementioned characterization techniques have been reported in the supplementary information, available online at stacks.iop.org/NANO/31/225708/mmedia.

Figure 1(c) shows the schematic illustration of TUNA setup whose description is given in the supplementary information. No preliminary treatment with silver paint (useful for creating electrical contacts on the ground) was carried out on the samples analyzed in this work.

Figure 1(d) show the test geometry adjusted for the healing experiments, whose details are provided in the supplementary information. Figure 1(e) show the epoxy samples before and after healing tests.

3. Results and discussion

Different techniques have been used to characterize the surface chemistry and CNT structure after covalent and non-covalent functionalization.

FTIR analysis has been accomplished in order to identify the functional groups anchored on the surface of the pristine (CNT) and modified (CNT–DDS and CNT–PDMS–Bz) CNTs (see figure 2(a)).

In the CNT spectrum, in addition to awaited signals C–C stretch at 1640 and 1543 cm^{-1}, attributable to skeletal vibrations from unoxidized domains, coming from the backbone of CNTs, we can also observe oxygenated functional groups (primarily hydroxyl and epoxide) that are present in non-negligible concentration. The bands at 3460 cm^{-1} (O–H stretching vibrations), at 1220 cm^{-1} (C–OH stretching vibrations), and at 1024 cm^{-1} (C–O stretching vibrations) confirm the presence of a different type of oxygen functionalities. The −OH groups are present in small quantities and are spaced. This can be deduced from the value of the stretching vibrations O–H and from the profile of this band which are typical of the hydroxyl group not bound to hydrogen or 'free' in the solid phase. The intermolecular hydrogen bonding between CNTs are strongly hampered by this spatial arrangement. As a result of this, it is possible to obtain a more effective distribution of CNTs within the polymeric matrix where the presence of aggregates is very limited, as is evident from the morphological analysis reported in this manuscript. The CNT–DDS spectrum shows the bands assigned to the stretching vibration of the sulfone group O=S=O (in DDS) at 1338 and 1146 cm^{-1}. The peaks at 1598 cm^{-1} and 3367 cm^{-1} correspond to the N–H bending and stretching vibration, respectively. The band at 1590 cm^{-1} can be assigned to the C=C in-plane deformation of the DDS benzene rings. The stretching vibration of the hydroxyl group is overlapped with stretching vibration of the amine group [55]. Moreover, we can observe for the covalently modified CNT–DDS a greater intensity of the C–C ring stretch signals (1600–1460 cm^{-1}) and a lower intensity of the signals related to the C–H aromatic stretches (3100–3000 cm^{-1}) (more pronounced for the CNT–PDMS–Bz nanofiller) with respect to what happens for the pristine CNT. Besides, the peak at 1273 cm^{-1} in the CNT–DDS spectrum due to the presence of the amino group N–H of DDS, the peak at 1101 cm^{-1} assigned to bond S=O of DDS ligand [34] and the peak corresponding to the bending vibration of p-disubstituted aromatic ring at 830 cm^{-1} demonstrate the presence of functional groups onto the CNT sidewall. There are three characteristic absorption bands in the FTIR spectrum of CNT–DDS. First, an absorption band at 3460 cm^{-1} attributed to the O–H stretching vibration derived from O–H groups on CNT [11] that is fairly broad, because the absorption band at about 3350 cm^{-1} is assigned to the N–H vibration of the amine group on DDS [56] combined with the O–H stretching vibration band of CNT. Typical FTIR signals of DDS such as absorption bands corresponding to C=C skeletal vibration at 1640 cm^{-1} and absorption bands of sulfone group O=S=O stretching vibration at 1140–1325 cm^{-1} are evident in the CNT–DDS spectrum giving a direct proof of the successful CNT functionalization with the DDS ligand. The structure of the benzoxazine terminated polydimethylsiloxane (PDMS–Bz) resin in the non-covalently functionalized CNT–PDMS–Bz is undoubtedly confirmed through FTIR analysis as shown in figure 2(a). The characteristic absorptions of the cyclic ether of benzoxazine ring structure appear at 1242 and 1012 cm^{-1} due to the asymmetric and symmetric stretching modes of C–O–C [57]. The presence of PDMS is proved by the

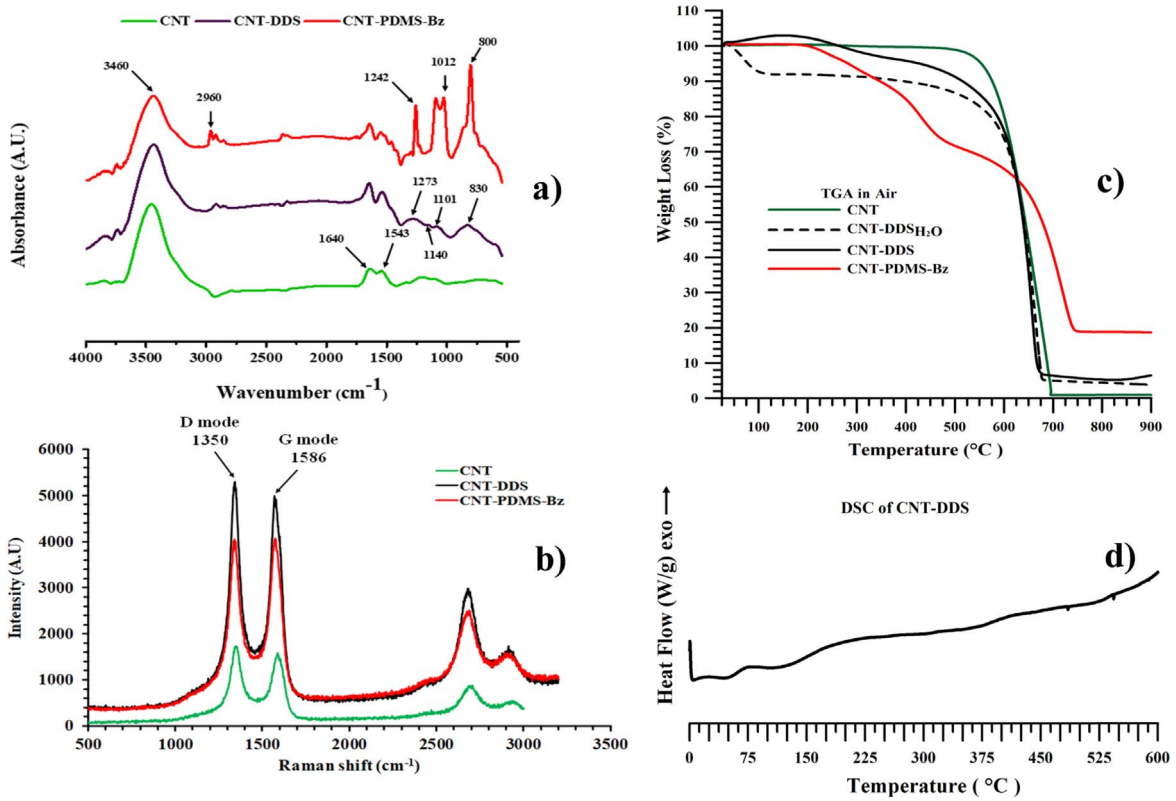

Figure 2. (a) FTIR spectra, (b) RAMAN spectra and (c) TGA curves of CNT, CNT–DDS, and CNT–PDMS–Bz nanofillers, (d) DSC curve of covalently functionalized CNT–DDS.

FTIR peaks at 800 cm^{-1} ($-CH_3$ rocking and Si–C stretching in Si–CH_3), 1020 cm^{-1} (Si–O–Si stretching), 1260 cm^{-1} (CH_3 deformation in Si–CH_3), and 2960 cm^{-1} (asymmetric CH_3 stretching in Si–CH_3) [58]. Additional proofs about the obtainment of the covalent and non-covalent functionalized CNTs come from Raman analysis that provides information on the degree of structural ordering and therefore the bonding states of carbons in the nanotube structure. Raman spectra collected both for pristine CNT and functionalized CNT–DDS and CNT–PDMS–Bz nanofillers (see figure 2(b)) exhibit two strong bands: the D mode (1350 cm^{-1}) known as defect-induced disorder mode which is related to local defects present in the carbon aromatic structure that originate from structural imperfections and is associated with the disordered sp^3 hybridized carbon network [59] and the tangential stretching G mode (1586 cm^{-1}) which is assigned to the C=C bond in the graphitic plane [60] and it is associated with the ordered sp^2 hybridized carbon network [30] in the investigated spectral range. The Raman spectrum of CNTs also exhibits two-phonon 2D (G′-band) modes at around 2600–2750 cm^{-1} corresponding to the overtone of the D-band, originated from a double-resonance process involving two-phonon and independent of the disorder [61]. The D-band is very useful for examining and monitoring structural changes resulting from the presence of defects or functional groups anchored to the surface of CNTs. The presence of a feature at ∼2900 cm^{-1}, observable in the functionalized CNT spectra, can be justified as a combination of two disorder-induced modes [62]. The ratio I_D/I_G can be used to obtain information regarding structural changes because of functionalization strategies and, usually, is used to qualitatively assess the content of structural defects in CNT [63]. In particular, a higher ratio I_D/I_G implies a greater presence of structural defects [64, 65] also providing indications on the degree of disorder in graphitic materials [66]. In our case, the high value of the ratio I_D/I_G can probably be attributed to the presence of functional groups covalently linked to the surface of the CNTs, as found by other authors for covalent bifunctionalizations [67, 68] or functional groups wrapped around the CNTs through a non-covalent functionalization, as also found by Cha *et al* for non-covalently functionalized CNTs [69].

The larger the I_D/I_G ratio is, the higher the defect level of the material is. In this study, for pristine CNT, the value of the I_D/I_G ratio was 1.19 which, although pretty small, is indicative of the fact that a quantity of defects as well as chemical species or functional groups attached to the nanofiller surface are still detectable even in the case in which the CNTs, like those used in this work, are commercially supplied as unfunctionalized CNT. Since, usually, the I_D/I_G ratio is taken as a measure of defect concentration, it has been argued that the G mode in the Raman spectra of CNTs originates from a defect induced double resonance scattering process [70]. As expected, the I_D/I_G ratio of the both covalently and non-covalently functionalized CNTs increases in comparison with unmodified CNT because of the two different approaches used for the functionalization (see RAMAN spectra reported in figure 2(b)). However, the I_D/I_G ratio is always higher for

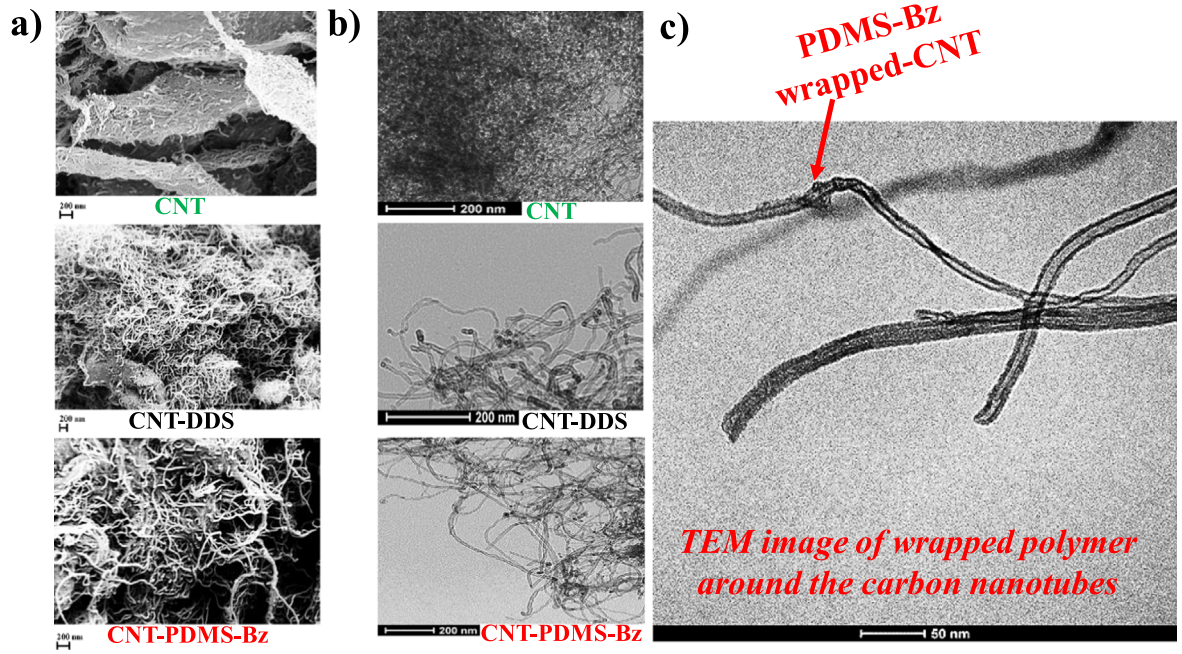

Figure 3. (a) FESEM images and (b) HRTEM images of CNT, CNT–DDS, and CNT–PDMS–Bz nanofillers, (c) HRTEM image of CNT–PDMS–Bz nanoparticles showing the wrapped polymer around the carbon nanotubes.

covalent functionalization, most likely because simultaneously surfactant molecules attach non-covalently to the CNT surface, thus leading to an increase in structural disorder [27]. Raman spectra show the G′-band (overtone of the D-band) and one weak feature at about 2950 cm^{-1}, observed beside the G′-band. The diazonium reaction of CNTs with DDS leads to a substantial increase of D band intensity relative to the G band (the I_D/I_G ratio increases) due to new defects in the CNT's surface indicating covalent bonding of DDS onto CNT surface. It is noteworthy that in the CNT–DDS nanofiller, although there is a major disorder due to the covalent functionalization (the intensity of D-band increases, while the intensity of G-band decreases), the surface modification took place without completely destroying the graphitic structure of the CNTs, preserving the sp^2 hybridization of carbon atoms. The sp^2 carbon network of the non-covalently functionalized CNT–PDMS–Bz is maintained also in covalently functionalized CNT–DDS and it is responsible for the high values of electrical conductivity obtained for both functionalized nanofillers. In particular, the DC conductivity of the nanocomposites containing functionalized CNTs reaches the high values of 8.81×10^{-3} S m^{-1} for TBD+1%CNT–DDS sample and 1.06×10^{-1} S m^{-1} for TBD+1%CNT–PDMS–Bz sample. It is worth noting that TBD+1%CNT nanocomposite shows a DC conductivity value of 2.92×10^{-1} S m^{-1} [8, 11, 49], which is comparable to that manifested by TBD+1%CNT–PDMS–Bz sample. In any case, both the functionalized nanofillers significantly affect the electrical behavior of the nanocomposites, making them conductive. This demonstrates that the two surface modification approaches (covalent and non-covalent) allow obtaining nanocomposites with good electrical properties while ensuring high mechanical and thermal performance, as described hereafter.

FESEM images giving the surface morphology of CNT, CNT–DDS and CNT–PDMS–Bz nanofillers are shown at the same magnification in figure 3(a).

This comparison shows that the functionalized CNTs (CNT–DDS and CNT–PDMS–Bz) seem better separated than unfunctionalized ones (CNT). In fact, the CNT nanoparticles appear entangled with each other showing a strong tendency to self-assemble into bundles due to van der Waals forces. Because of the functionalization, a more clear distribution of CNTs is observed. This effect is more evident for the CNT–PDMS–Bz, obtained through non-covalent supramolecular adsorption of functional molecules onto the CNT walls. This is most likely due to the surfactant absorption action that hampers the re-agglomeration and widens the spaces between carbon nanofillers, finally disentangling the individual nanotubes from the bundle. Besides, the morphology of the functionalized nanofillers remains intact: in fact, no CNT destruction is observed thus giving proof that the CNT are capable of resisting the process of functionalization. These results demonstrate that the covalent and non-covalent functionalizations avoid the CNT aggregates, thus leading to nanocomposites with improved functional and structural properties. The HRTEM images show the morphology of the functionalized carbon nanotubes CNT–DDS and CNT–PDMS–Bz compared with the pristine CNT (see figure 3(b)). From these images, we have the confirmation that the modified CNTs are better separated compared to pristine ones. Furthermore, it can be clearly observed that the pristine nanotubes CNT exhibit smaller diameters compared with the functionalized ones CNT–DDS and CNT–PDMS–Bz. This reconfirms the success of the performed functionalizations. In particular, the HRTEM image at higher magnification of the non-covalently functionalized nanofillers CNT–PDMS–Bz

clearly shows the wrapped polymer around the CNTs (see figure 3(c)).

TGA measures the decrease in sample mass over time as the temperature changes. TGA curves in air for CNT, CNT–DDS and CNT–PDMS–Bz nanofillers are shown in figure 2(c). We can see that the unfunctionalized CNT are stable up to about 525 °C and at this temperature both the CNT–DDS and CNT–PDMS–Bz hybrid nanoparticles show a weight loss attributable to the degradation of the functional groups grafted or physically immobilized on the CNT surface. TGA measurements in air show that CNTs have a different thermogravimetric pattern depending on the presence and type of functionalization used.

In particular, in the case of CNT–DDS nanofiller (see black dotted curve), there is a weight loss of about 5% due to the presence of moisture content as also observable in the DSC thermogram (see figure 2(d)) performed on the same sample. Concerning the profile of the TGA curve at temperature lower than 100 °C, affected by the weight loss of the adsorbed moisture, a similar change in the TGA curve profile due to the dissipation of absorbed water was found by Hou *et al* [71] for microcages of MnO@C-700 fabricated through a facile bio-inspired synthesis strategy for highly reversible Li storage. The profile of the TGA curve of the sample CNT–DDS changes in the expected direction when the sample is subjected to heat treatment for 24 h at 100 °C under vacuum. After this treatment, the weight loss due to the moisture completely disappears, while it is evident that the covalently functionalized CNTs react towards the oxygen of the air, which produces an initial increase of about 2.5% in weight. The authors of [71] also found weight gains in TGA curve profile due to oxidation reactions. This weight increase is lost at the temperature of about 250 °C, after which a single weight drop, which is completed at about 700 °C, is observed. The residues at the end of the TGA analysis were 6% and 18% for the functionalized carbon nanotubes CNT–DDS and CNT–PDMS–Bz, respectively, while a residue less than 2% is found for the pristine CNT. The loss factor, tanδ, and storage modulus, E′ (MPa), of the uncharged formulation (TBD) and samples filled with a concentration of 1% by wt of nanofiller (TBD+1% CNT, TBD+1%CNT–DDS, TBD+1%CNT–PDMS–Bz) are shown in figures 4(a), (b), respectively.

For all the investigated samples, we can observe E′ storage modulus values higher than 2000 MPa between −100 °C and 100 °C. A sluggish and increasing reduction of E′ up to 50 °C, followed by a nearly constant value between 50 °C and 200 °C before the principal drop, due to the glass transition temperature Tg, which is evident between 200 °C ÷ 300 °C, is detectable in figure 4(b), and further confirmed in figure 4(a). The glass transition of the sample (α transition), corresponding to the highest peak, is positioned at 262 °C for the uncharged resin TBD, 261 °C for the sample TBD+1% CNT, 260 °C for the sample TBD+1%CNT–DDS and 283 °C for the sample TBD+1%CNT–PDMS–Bz. Considering the concentration of 1% by weight of CNTs, the covalent functionalization does not affect the Tg value of the sample TBD +1%CNT–DDS, with respect to the nanocomposite with unfunctionalized CNTs (260 °C and 261 °C), whereas a strong increase in Tg value is detected for the sample filled with CNTs non-covalently functionalized (CNT–PDMS–Bz). As regards the tanδ values, it is worth to observe that the profiles of the samples containing incorporated functionalized CNTs are composed of two overlapped peaks. These two peaks are indicative of a lower temperature glass transition, beside the main transition, which is located at the same temperature of the pristine resin for the sample with CNTs covalently functionalized and at higher temperature for the sample with CNTs non-covalently functionalized. The presence of a secondary peak, active at a lower temperature, in the loss factor suggests the presence of a fraction of amorphous phase with higher mobility due to a different degree of crosslinking. The position and the intensity (height) of this secondary peak are depending on the nature of the functionalization. In particular, the presence of the –DDS groups determines a fraction of resin at lower density network with a lower Tg. This result is compatible with a poor reactivity of the $-NH_2$ groups with the epoxy precursor and a partially interruption of the crosslinking at the interface with the wall of the CNTs. Of course, this determines a decrease of the intensity in main peak, which is located at the same temperature of the unfilled resin. The phase at lower glass transition temperature determines a lower modulus with is counterbalanced by the tendency to increase the modulus, due to the covalent functionalization. The global result is the same value in the modulus of the sample containing unfunctionalized nanotubes. It is worth noting that also nanotubes sold as unfunctionalized always show a small fraction of functional groups [11]. For the nanocomposite containing non-covalently functionalized CNTs, the secondary peak (at lower temperature) is less intense and shifted at higher temperature. This behavior is indicative of physical adsorptions, which leave unchanged the crosslinking density around the interface between CNTs and matrix; in addition, the groups non-covalently bonded around the wall of CNTs prevent, by shielding, the chemical interactions between the few functional groups always present on the non-functionalized nanotubes and the epoxy precursor. This results in an increase in the main transition peak and a decrease in the storage modulus. The unfilled resin TBD show the height value of the main peak equal to 0.52, whereas for the nanocomposites it is between 0.45 and 0.48. From this, it is clear that the nanocomposites manifest more toughened behavior than the unfilled resin TBD. The presence of the secondary peaks in the nanocomposites containing incorporated functionalized CNTs suggests a broader distribution of relaxation times, most likely attributable to more nano-particle/polymer interactions, with phases at the interface characterized by changed mobility of the molecular segments. The formation of a few nm thick intermediate layer on the resin-filler interface, as it has already been reported in [72–76], presumably takes place before the sample is completely cured, thus leading to the increase of the secondary peak shown in figure 4(a). The addition of the filler determines a decrease of the reaction enthalpy and the curing degree, as expected in consideration of the previous observations. Figures 4(c) and (d) highlight the difference among samples filled with

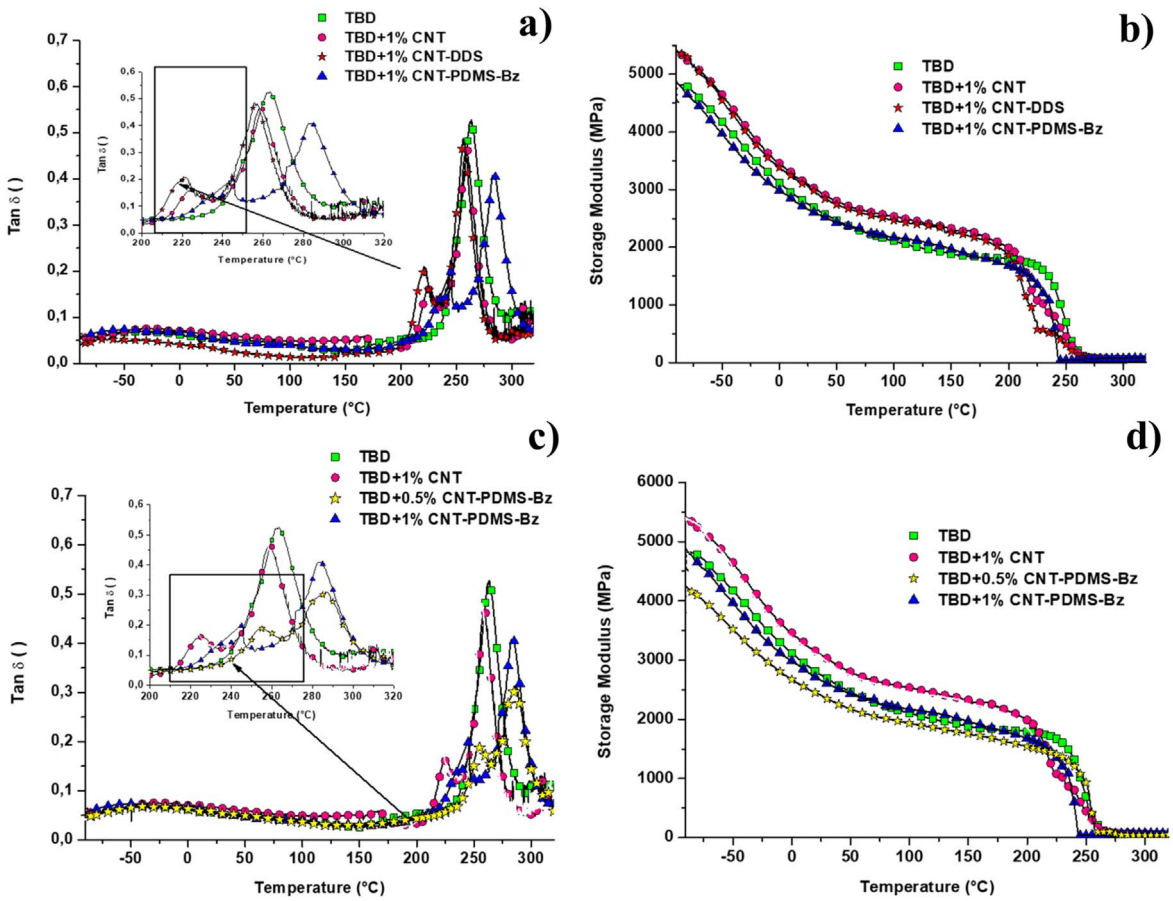

Figure 4. (a) Loss factor (tanδ) and (b) storage modulus of the uncharged resin TBD and nanocomposites TBD+1% CNT, TBD+1%CNT–DDS, TBD+1%CNT–PDMS–Bz, (c) loss factor (tanδ) and (d) storage modulus of the uncharged resin TBD and nanocomposites TBD+1% CNT, TBD+0.5%CNT–PDMS–Bz, TBD+1%CNT–PDMS–Bz.

different percentage of non-covalently functionalized CNTs. It is possible to observe, as expected, that an increase of CNT percentage determines an increase in the storage modulus due to the increase of the interactions at the interface between matrix and CNT wall; whereas the profile of tan δ highlights a less toughened behavior with respect to higher percentages of functionalized CNTs.

Summarizing, both the functionalized CNTs form in the resin a second phase with different crosslinking density and with different values of Tg depending to the nanofiller nature. In particular, the CNTs covalently functionalized with DDS hardener ligand allow greater interaction with the part of the matrix that presents higher mobility of chain segments. In any case, the Tg values of the analyzed nanocomposites range from 260 °C to 280 °C and the storage modulus is higher than 2000 MPa up to 150 °C. These results prove that all the analyzed formulations can be used for structural and functional applications.

Figures 5(a), (b) shows the TGA thermograms in air and in inert (N_2) atmosphere of the TBD matrix and epoxy nanocomposites loaded with unfunctionalized and functionalized CNTs before curing cycle (uncured samples). Regarding CNT–DDS based nanocomposites, two formulations TBD+1%CNT–DDS and TB+1%CNT–DDS, differing only for the presence in the epoxy mixture of DDS curing agent (D), were prepared. The planning of these nanocomposites was aimed at evaluating the effect of the DDS hardener agent covalently bonded to the CNT surface on the nanocomposite thermal stability. In the air, we can observe a two-step thermal degradation process for all epoxy samples. This means that the addition of carbon nanofillers in the resin does not greatly affect the degradation mechanism of the formulation. From a careful observation of the TGA thermograms both in air and in nitrogen, we can clearly see that, in the first stage of the degradation process, all the nanocomposites are less thermostable than the uncharged TBD resin. Furthermore, it is worth noting that at 120 °C an extremely limited amount of material starts to degrade due to the degradation of the reactive diluent (B) [49] (see the TGA curves in figures 5(a), (b) related to the liquid mixtures, before the curing process), which appears more evident for the sample TB+1%CNT–DDS containing only the diluent (B) in absence of DDS curing agent (D).

A noteworthy aspect concerns a different mass loss at the end of the first degradation stage for the analyzed samples, which results in a higher percentage in nitrogen than that recorded in the air. Thus, the nanofiller does not affect the first stage, whereas it instead becomes relevant in the second stage of degradation. The epoxy formulations, after a heat treatment in an oven up to 200 °C, were subjected to TGA in air (see

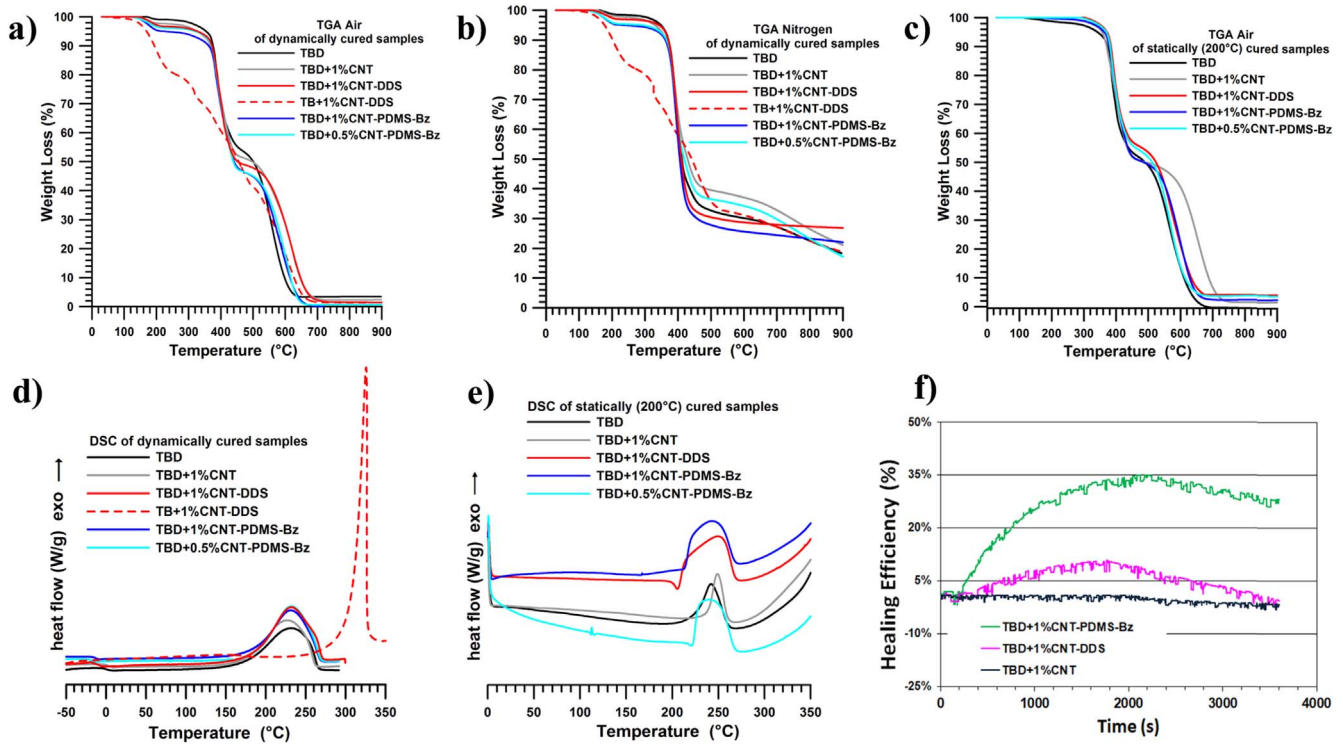

Figure 5. (a) TGA curves in air and (b) TGA curves in nitrogen of dynamically cured epoxy samples, (c) TGA curves in air of statically (200 °C) cured epoxy samples, (d) DSC curves of dynamically cured epoxy samples (first run), (e) DSC curves of statically (200 °C) cured epoxy samples (second run), (f) healing efficiency of the formulations TBD+1%CNT–PDMS–Bz, TBD+1%CNT–DDS and TBD+1%CNT.

Table 1. DC values of the analyzed samples dynamically and statically cured.

Sample	Curing degree DC (%) DSC cure (samples dynamically cured)	Curing degree DC (%) oven cure (200 °C) (samples statically cured)
TBD	100	95
TBD+1%CNT	100	95
TBD+1%CNT–DDS	100	87.5
TBD+1%CNT–PDMS–Bz	100	89
TBD+0.5%CNT–PDMS–Bz	100	89

figure 5(c)). We can observe that the temperature of the beginning of the degradation for the unloaded TBD formulation is the same at which the TGMDA resin alone (T) begins to degrade, i.e. 320 °C. This remarkable result proves that the thermal stability of the BDE diluent, when it is part of the crosslinked resin, is guaranteed up to 320 °C [49]. An extremely important result is that all nanocomposites, after a curing process, when compared to the unfilled resin TBD, are more thermostable in the first degradation stage (see figure 5(c)), thus proving that the functionalizations imparted to the CNTs have been effective in the thermal stabilization process of the epoxy formulation. In this work, the curing degree (DC) of the different formulations was evaluated in a dynamic and isothermal regime by DSC analysis [48, 49] using calorimetric data. Detailed information about the two different experimental procedures that were used to obtain DSC results has been reported in the supplementary information. Figures 5(d), (e) shows the DSC curves of dynamically cured epoxy samples (first run) and the DSC curves of statically (200 °C) cured epoxy samples (second run), respectively.

Since DDS is known as an efficient hardener for epoxy matrix and hence an influence of the amine groups on the resin crosslinking process is expected, in this work we have made a preliminary assessment aimed at obtaining information about the behavior of DDS ligand covalently attached to the CNT surface in activating the cross-linking reaction in the epoxy resins. The epoxy sample named TB+1%CNT–DDS, where the DDS added as a curing agent in the stoichiometric ratio was completely absent, has been prepared. The preliminary calorimetric results so far obtained on the dynamically cured sample TB+1%CNT–DDS (see figure 5(d)) shows that in the range 270 °C–350 °C an intense peak whose enthalpy content is $(\Delta H_T) = 695\,J\,g^{-1}$ can be detected. Although this result could have suggested the effectiveness of the DDS to act as a crosslinking agent, despite being present in reduced quantity directly connected to the CNTs, however, this has not actually occurred, since the calorimetric trace of

the epoxy system containing only TGMDA resin and BDE diluent (not reported here) shows the same intense peak and the same temperature range, which can be associated with the classical homopolymerization phenomena due to free radicals activated during the thermal degradation of the material. Table 1 shows the DC values of the samples dynamically and statically cured.

The DC values were found to be higher than 87.5% even for the samples statically cured. More specifically, the DC values of the functionalized CNT–DDS and CNT–PDMS–Bz based nanocomposites are lower than the unloaded resin TBD and unfunctionalized CNT based sample for which the DC reaches the value of 95%. In particular, for the TBD+1% CNT–DDS sample, the DC value is 87.5%, whereas for both epoxy samples loaded with 0.5% and 1% by wt of CNT–PDMS–Bz the DC value is 89%. These results highlight that the functionalized nanofillers interrupt the cross-linking reaction during the curing process, thus leading to a decrease in the Tg, as previously discussed. In particular, in our system, the addition of the nanofiller does not determine a real lowering of the Tg but rather the creation of a transition at lower temperatures. This transition suggests the presence of a phase characterized by greater movements of chain portions, intimately connected to the filler. The increased mobility allows a better transfer of load on the filler, as shown by the value of storage modulus, which is comparable or higher than that of uncharged resin. In any case, the DC values recorded for the functionalized CNTs are anyhow acceptable for aeronautic epoxy formulations.

Figure 5(f) shows the healing efficiency of the TBD+1% CNT, TBD+1%CNT–DDS and TBD+1%CNT–PDMS–Bz epoxy samples. The healing efficiency evaluation is reported in the supplementary information.

Results reported in figure 5(f) highlight that the self-healing ability of the three tested samples is quite different. The TBD+1%CNT–PDMS–Bz sample shows a well-defined maximum in the healing efficiency, defined as the percentage of elastic modulus recovered, followed by a very slight drop. The TBD+1%CNT–DDS sample shows a small recovery followed by a quick drop probably due to the crack propagation caused by the cyclic fatigue stress. The small recovery is associated with the poor activity of NH_2 groups during the crosslinking reactions; this condition enables reversible self-healing interactions via hydrogen bonds. No healing efficiency is observed for the TBD+1%CNT sample (reference sample) highlighting that unfunctionalized CNT alone are not able to give self-healing functionalities to the thermosetting system [11]. The noteworthy result is that the functionalization has proved to be a winning strategy in activating self-healing efficiency. In particular, however, the efficiency value recorded for the nanocomposite TBD+1%CNT–DDS loaded with covalently functionalized CNTs is much lower (∼10%) than that recorded for the nanocomposite TBD+1%CNT–PDMS–Bz loaded with CNTs functionalized following the non-covalent approach that instead reaches values up to ∼35%. These results clearly show that: (a) both covalently CNT–DDS and non-covalently CNT–PDMS–Bz functionalized CNTs turned out to be really effective in activating self-repair mechanisms in the epoxy matrix, contrary to what occurs in the case of unfunctionalized CNT that do not confer any self-healing efficiency; (b) non-covalently functionalized CNT–PDMS–Bz embedded in the epoxy formulation allow to obtain higher efficiency values compared to covalently functionalized CNT–DDS. Thus, the polymer-wrapped CNTs obtained by non-covalent functionalization have led to an increase in the self-repairing efficiency of approximately 350%. This relevant result can be explained because in the non-covalent functionalization with conjugated polymers, chemical groups are attached without interrupt the bonding network of the CNTs, whereas covalent functionalization by introducing atomic defects and internal stress can lead to the deterioration of the mechanical properties and then to the decrease of the healing efficiency. The intense interactions between the CNTs and the PDMS–Bz network, whose strength is intimately correlated with the chemical structure of the precursor, give rise to hybrid nanocomposites with exceptional properties and with a significant thermo-mechanical reinforcement. The FESEM analysis aimed at assessing the state of nanofiller dispersion was carried out on etched samples. Figures 6(a), 7(a), 8(a) show FESEM images at the same magnification of the fracture surface of the TBD +1%CNT, TBD+1%CNT–DDS, and TBD+1%CNT–PDMS–Bz nanocomposites, respectively. The functionalized nanofillers CNT–DDS and CNT–PDMS–Bz exhibit good dispersion in the epoxy resin also for load percentages up to 1% by wt. The uniform dispersion of the functionalized CNTs inside the resin is fundamental to obtain an effective reinforcing effect. The presence of the functional groups prevents CNTs from agglomerating through π–π interactions leading to strong interfacial interactions between carbon nanofiller and the epoxy matrix. In this work, an additional interface between the filler and the matrix was obtained following the addition of the functionalized fillers inside the resin. In particular, in the case of the CNT–DDS, the interface was formed thanks to the covalent bonds with epoxy groups in the host matrix through the amino groups of the DDS ligand, whereas instead, in the case of the CNT–PDMS–Bz filler, it it occurred thanks to numerous supramolecular interactions. FESEM analysis shows that unfunctionalized nanofillers CNT have a greater tendency to agglomerate forming bundles, or entanglements of nanotubes more readily with respect to functionalized nanofillers CNT–DDS and CNT–PDMS–Bz. The sonication positively influenced the final dispersion of the nanofillers leading to a better disentanglement of the CNT bundles. In addition, the dispersion of CNTs after chemical modification and wrapping polymer onto the CNT structure show considerable improvements (see FESEM images in figures 7(a) and 8(a) of the nanocomposites TBD+1%CNT–DDS and TBD+1%CNT–PDMS–Bz, respectively). An aspect of considerable importance, closely related to the matrix-nanofiller interaction, emerges from the comparison in morphological peculiarities of the three formulated nanocomposites. In fact, from the micrographs it is clear that the unfunctionalized CNTs seem less bound to the epoxy matrix than the functionalized CNTs despite the same etching procedure was used for the three different nanocomposites.

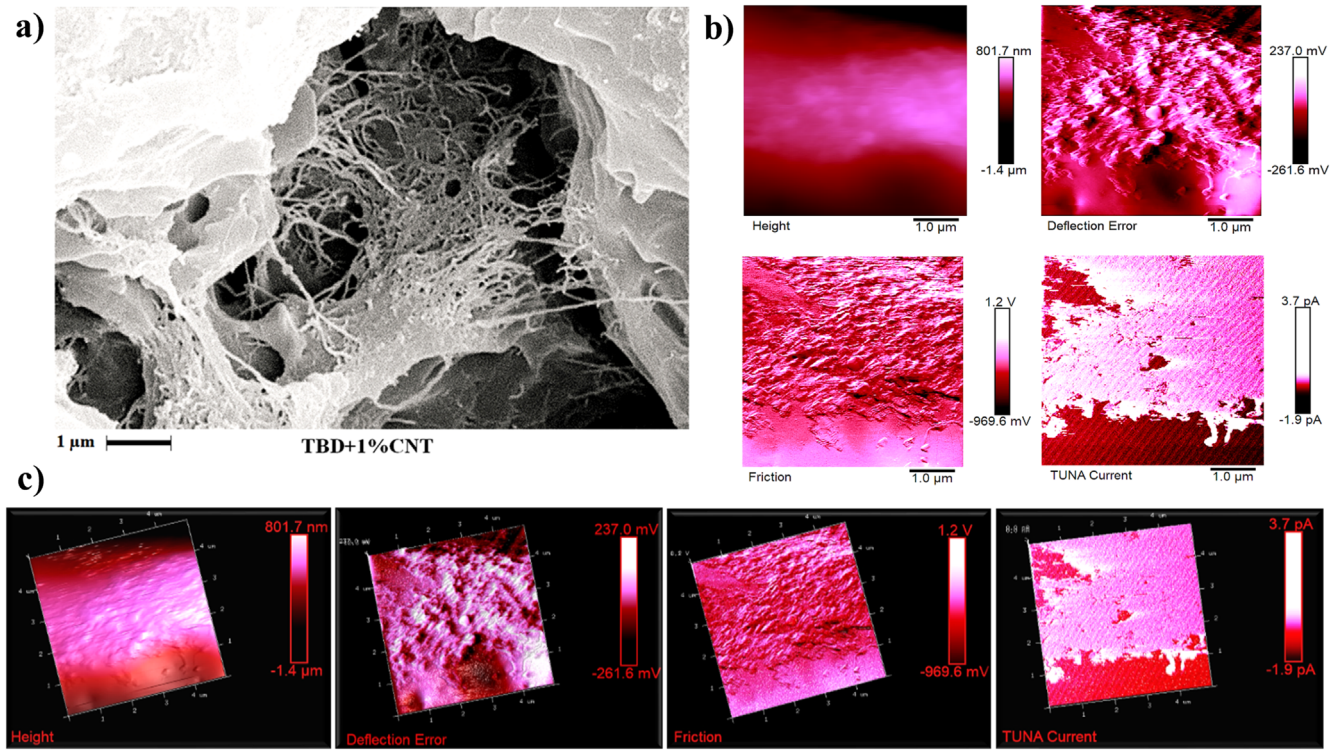

Figure 6. Morphological analysis of the TBD+1%CNT etched fracture surface: (a) FESEM image, (b) the four TUNA–AFM image types, and (c) the corresponding four three-dimensional TUNA–AFM images.

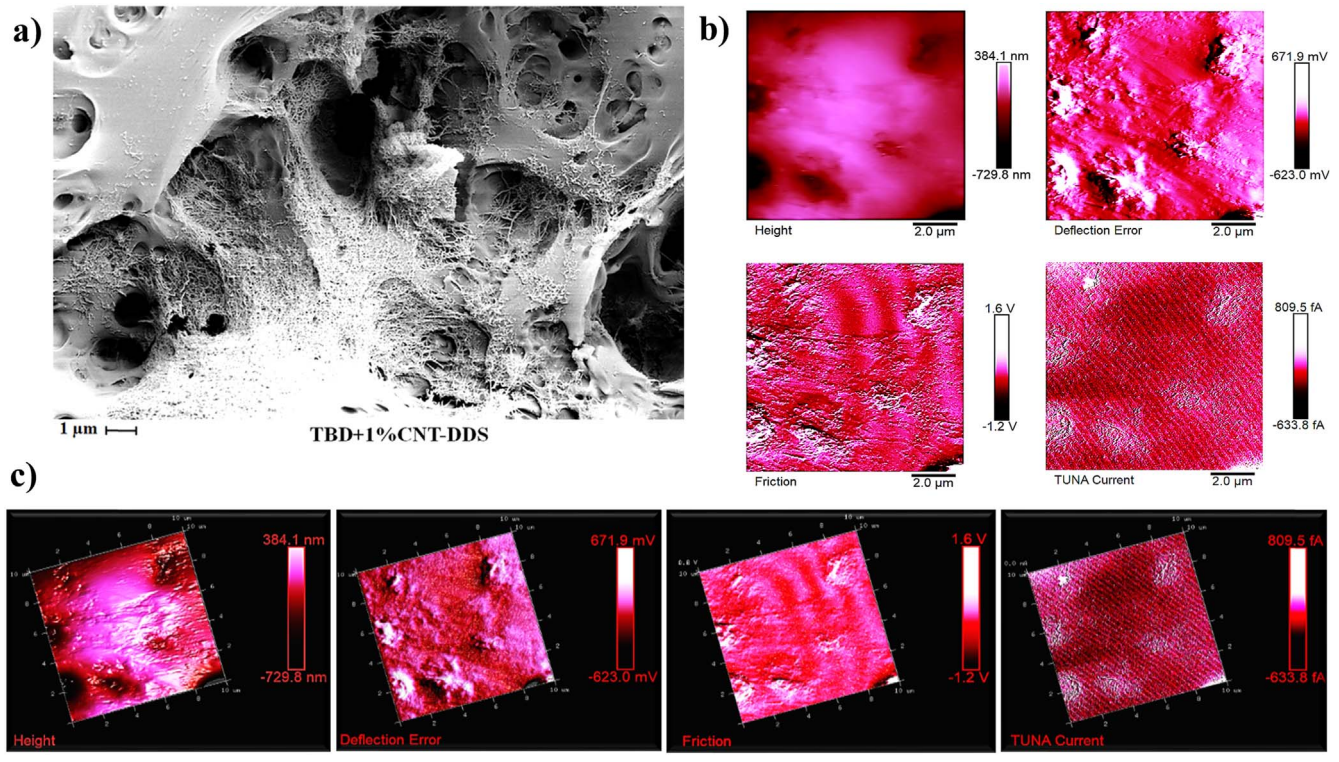

Figure 7. Morphological analysis of the TBD+1%CNT–DDS etched fracture surface: (a) FESEM image, (b) the four TUNA–AFM image types, and (c) the corresponding four three-dimensional TUNA–AFM images.

However, a continuous network of CNTs, responsible for the electrical conductivity of the samples, is clearly observable in all three nanocomposites, particularly evident in several dark areas of the FESEM images where the etching procedure is very effective. Figures 6(b), 7(b), and 8b show the TUNA–AFM micrographs and figures 6(c), 7(c) and 8(c) the corresponding three-dimensional profiles collected on etched samples TBD+1%CNT, TBD+1%CNT–DDS, and

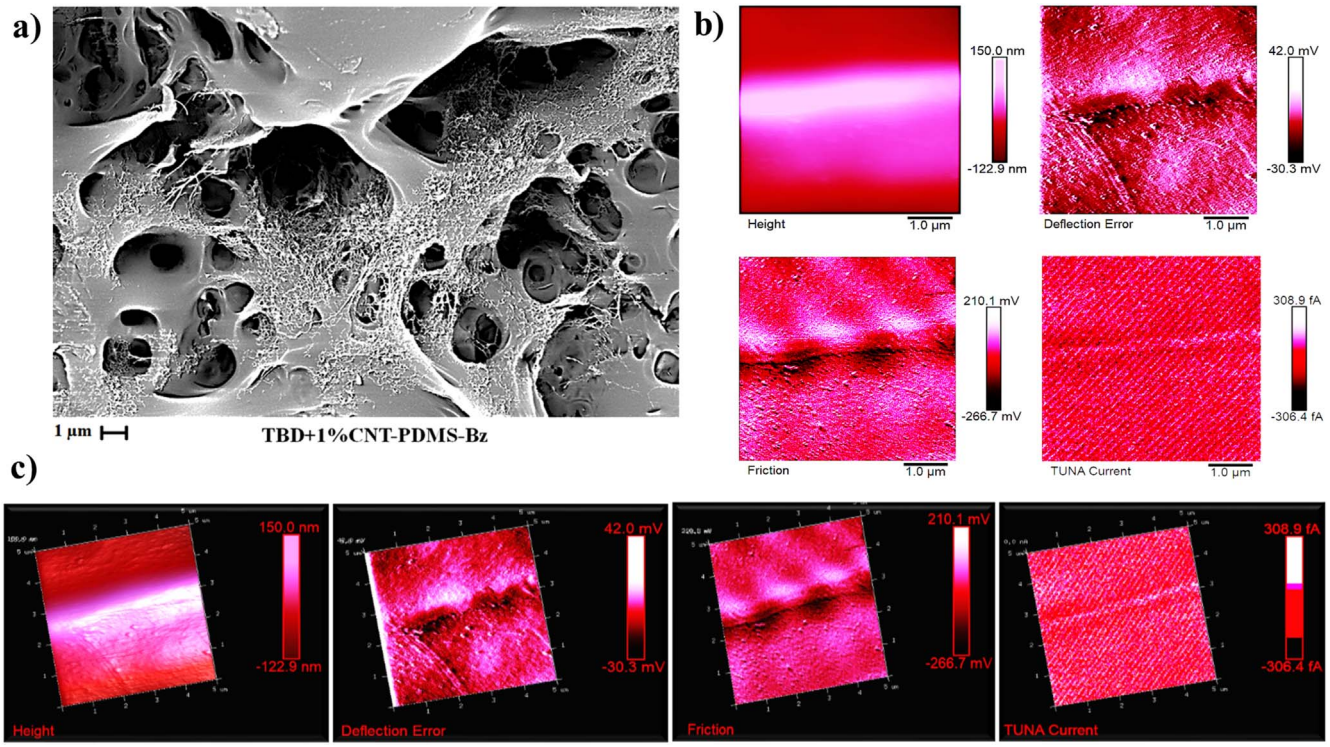

Figure 8. Morphological analysis of the TBD+1%CNT–PDMS–Bz etched fracture surface: (a) FESEM image, (b) the four TUNA–AFM image types, and (c) the corresponding four three-dimensional TUNA–AFM images.

TBD+1%CNT–PDMS–Bz, respectively. Four TUNA–AFM images, namely height (or topography) image, deflection error image, friction image, and tuna current image are shown for each nanocomposite. The TUNA–AFM images, thanks to the high spatial resolution together with the several modes of detection of different physical properties through a simultaneous mapping of the topography and the nanometric current distribution, allow to correlate a position of the sample with its electrical properties. In this paper, the four TUNA–AFM images (see figures 6(b), (c), 7(b), (c) and 8(b), (c)) allow the morphological characteristics of the three nanocomposites to be more clearly identified and are effective in helping to understand more fully the electrical properties observed by virtue of the interrelating information they provide. In particular, we can distinctly detect the conductive network of CNTs firmly attached to the resin, mainly in 2D and 3D TUNA current pictures. In fact, the homogeneous distribution of the CNTs on the surface of the sample, although viewable in almost all the images, is much more evident in the TUNA current images as they show a greater contrast of colors which is associated with the morphological characteristics of the nanoparticles. When a measurable current is recorded, it is possible to correlate the topography with the high current sample areas. In this regard, in the TUNA current images, the higher brightness in the light pink color is undoubtedly attributable to the conductive carbon nanoparticles. This is a tangible proof of their high electrical conductivity. Instead, the regions of the sample with reduced conductivity appear with a darker and less intense color.

The current profile also allows the detection of domains with different brightness that are associated with different current values. In fact, TUNA current images in figures 6(b), 7(b), and 8(b) clearly show that the nanocomposites are intrinsically conductive because for the samples TBD+1% CNT, TBD+1%CNT–DDS and TBD+1%CNT–PDMS–Bz low current values ranging from 1.9 pA to 3.7 pA, 633.8 fA to 809.5 fA and 306.4 fA to 308.9 fA were measured, respectively. The detection of such low current values unquestionably proves the relative high values of the electrical conductivity (2.92×10^{-1} S m^{-1} for TBD+1%CNT, 8.81×10^{-3} S m^{-1} for TBD+1%CNT–DDS and 1.06×10^{-1} S m^{-1} for TBD+1%CNT–PDMS–Bz) and the well-defined conductive pathways closely related to the effective dispersion of the conductive nanoparticles. This is evident by observing the marked chromatic variations associated with the most conductive areas of the samples where the presence of carbon nanofillers that ensure the efficacious transport of the electrical properties on the surface of the resin is really relevant.

4. Conclusions

This study proves effective approaches for enhancing the interactions of CNTs with epoxy matrix in order to enable a much better dispersion within the resin formulation. The CNT functionalization through covalent and physical bonds with the cross-linked epoxy matrix has been studied to clarify the role of the matrix-filler interphase in the enhancement of mechanical, thermal and electrical properties of the resulting

nanocomposites. The covalent functionalization has been performed using as a functional group the same hardener agent employed to solidify the epoxy matrix. This assures very effective compatibility of the nanofiller with the hosting epoxy matrix. The results demonstrate that the CNT functionalization facilitates the transfer of both mechanical load and thermal energy across the matrix-filler interface. Reversible attractive interactions are capable to confer self-healing efficiency to the nanocomposites containing embedded functionalized CNTs. The performed functionalizations were successfully proved by FTIR and Raman spectroscopies and the effectiveness of the dispersion attributable to the functionalization is clearly visible from the FESEM images. The adopted unfilled resin TBD has a volume conductivity at room temperature of about $6.00 \times 10^{-14}\,\mathrm{S\,m^{-1}}$, whereas TBD + 1%CNT nanocomposite shows a DC conductivity value of $2.92 \times 10^{-1}\,\mathrm{S\,m^{-1}}$. The incorporation of CNT–PDMS–Bz and CNT–DDS functionalized nanofillers has a strong impact on the electrical behavior of the nanocomposites leading to samples TBD + 0.5%CNT–PDMS–Bz and TBD + 1%CNT–PDMS–Bz characterized by DC conductivities of $1.65 \times 10^{-2}\,\mathrm{S\,m^{-1}}$ and $1.06 \times 10^{-1}\,\mathrm{S\,m^{-1}}$ respectively, and sample TBD + 1%CNT–DDS characterized by DC conductivity of $8.81 \times 10^{-3}\,\mathrm{S\,m^{-1}}$. The DMA shows that all nanocomposites can be used for various structural applications as they provide high values of the storage modulus and glass transition temperature (Tg). TGA shows a greater thermostability of the nanocomposites compared to unfilled epoxy matrix TBD, also highlighting a stabilizing effect of the nanofillers in the first stage of the degradation. The non-covalent approach through the polymer-wrapped CNTs, maintaining the CNT intrinsic properties with numerous supramolecular interactions, allows obtaining the highest healing efficiency value. The increase in the self-healing efficiency of about 350% represents a very relevant result that can be explained because conjugated polymer (PDMS–Bz) acts as excellent wrapping material for the non-covalent CNT functionalization because of π–π stacking and van der Waals interactions between the PDMS–Bz and the CNT surface. The TUNA–AFM technique has demonstrated its effectiveness in detecting the conductive pathways within the epoxy system loaded with CNTs, both unfunctionalized and functionalized. In this way, it has also proved to be an exceptional tool for evaluating the success of a functionalization. Furthermore, the technique has allowed us to identify the nanometric distribution of carbon nanoparticles, also highlighting their strong interconnections with the host matrix that are responsible for the highly performing properties of the formulated nanocomposites. TUNA images highlight that two different functionalizations were successfully performed giving rise to interpenetrated conductive epoxy structures. Summing-up, unique and out-performing properties have been demonstrated for CNTs interacting with conjugated polymer and for the surfaces of CNTs chemically modified by DDS curing agent, thus opening the way for new applications of these hybrid materials.

Acknowledgments

The research leading to these results has received funding from the European Union's Horizon 2020 research and innovation programme under grant agreement No. 760940—MASTRO.

The authors also wish to thank the 'Région Wallonne' and the European Community for general support in the framework of FP7 ('IASS' project), the Interreg V program ('BIOCOMPAL' project), the FEDER 2014–2020 program ('HYBRITIMESURF' and 'MACOBIO projects). They also thank Oltea Murariu and Dr Ludovic Dumas for their help in the preparation of PDMS-Bz.

Conflict of interest

The authors declare no conflict of interest.

ORCID iDs

Marialuigia Raimondo https://orcid.org/0000-0003-1963-9472

References

[1] Iijima S 1991 Helical microtubules of graphitic carbon *Nature* **354** 56–8

[2] Lavall R L, de Sales J A, Borges R S, Calado H D R, Machado J C, Windmöller D, Silva G G, Lacerda R G and Ladeira L O 2010 Thermoplastic polyurethane and multi-walled carbon nanotubes nanocomposites for electrostatic dissipation *Quim. Nova* **33** 133–40

[3] Ma P-C, Siddiqui N A, Marom G and Kim J-K 2010 Dispersion and functionalization of carbon nanotubes for polymer-based nanocomposites: a review *Composites* A **41** 1345–67

[4] Qian D, Wagner G J, Liu W K, Yu M-F and Ruoff R S 2002 Mechanics of carbon nanotubes *Appl. Mech. Rev.* **55** 495–533

[5] Yang S-Y, Ma C-C M, Teng C-C, Huang Y-W, Liao S-H, Huang Y-L, Tien H-W, Lee T-M and Chiou K-C 2010 Effect of functionalized carbon nanotubes on the thermal conductivity of epoxy composite *Carbon* **48** 592–603

[6] Romano V, Naddeo C, Guadagno L and Vertuccio, L 2015 Thermal conductivity of epoxy resins filled with MWCNT and hydrotalcite clay: Experimental data and theoretical predictive modeling *Polym. Compos.* **36** 1118–23

[7] Romano V, Naddeo C, Vertuccio L, Lafdi K and Guadagno L 2017 Experimental evaluation and modeling of thermal conductivity of tetrafunctional epoxy resin containing different carbon nanostructures *Polym. Eng. Sci.* **57** 779–86

[8] Guadagno L, Naddeo C, Raimondo M, Barra G, Vertuccio L, Russo S, Lafdi K, Tucci V, Spinelli G and Lamberti P 2017 Influence of carbon nanoparticles/epoxy matrix interaction on mechanical, electrical and transport properties of structural advanced materials *Nanotechnology* **28** 094001

[9] Guadagno L, Naddeo C, Raimondo M, Barra G, Vertuccio L, Sorrentino A, Binder W H and Kadlec M 2017 Development of self-healing multifunctional materials *Composites* B **128** 30–8

[10] Ardjmand M, Omidi M and Choolaei M 2015 The effects of functionalized multi-walled carbon nanotube on mechanical properties of multi-walled carbon nanotube/epoxy composites *Orient. J. Chem.* **31** 2291–301
[11] Guadagno L, Raimondo M, Vertuccio L, Naddeo C, Barra G, Longo P, Lamberti P, Spinelli G and Tucci V 2018 Morphological, rheological and electrical properties of composites filled with carbon nanotubes functionalized with 1-pyrenebutyric acid *Composites* B **147** 12–21
[12] Gantayat S, Rout D and Swain S K 2017 Mechanical properties of functionalized multiwalled carbon nanotube/epoxy nanocomposites *Mater. Today: Proc.* **4** 4061–4
[13] Naddeo C, Vertuccio L, Barra G and Guadagno L 2017 Nano-charged polypropylene application: realistic perspectives for enhancing durability *Materials* **10** 943
[14] Thostenson E T, Ren Z and Chou T-W 2001 Advances in the science and technology of carbon nanotubes and their composites: a review *Compos. Sci. Technol.* **61** 1899–912
[15] Ajayan P M, Schadler L S and Braun P V 2003 *Nanocomposite Science and Technology* (Weinheim: Wiley) p 77
[16] Coleman J N, Khan U and Gun'ko Y K 2006 Mechanical reinforcement of polymers using carbon nanotubes *Adv. Mater.* **18** 689–706
[17] Guadagno L, Naddeo C, Raimondo M, Gorrasi G and Vittoria V 2010 Effect of carbon nanotubes on the photo-oxidative durability of syndiotactic polypropylene *Polym. Degrad. Stab.* **95** 1614–26
[18] Vertuccio L, Vittoria V, Guadagno L and De Santis F 2015 Strain and damage monitoring in carbon-nanotube-based composite under cyclic strain *Composites* A **71** 9–16
[19] Kathi J, Rhee K-Y and Lee J H 2009 Effect of chemical functionalization of multi-walled carbon nanotubes with 3-aminopropyltriethoxysilane on mechanical and morphological properties of epoxy nanocomposites *Composites* A **40** 800–9
[20] Lipinska M E, Rebelo S L H, Pereira M F R, Gomes J A N F, Freire C and Figueiredo J L 2012 New insights into the functionalization of multi-walled carbon nanotubes with aniline derivatives *Carbon* **50** 3280–94
[21] Ménard-Moyon C, Fabbro C, Prato M and Bianco A 2011 One-pot triple functionalization of carbon nanotubes *Chem. Eur. J.* **17** 3222–7
[22] Bottini M, Bruckner S, Nika K, Bottini N, Bellucci S, Magrini A, Bergamaschi A and Mustelin T 2006 Multi-walled carbon nanotubes induce T lymphocyte apoptosis *Toxicol. Lett.* **160** 121–6
[23] Saeb M R, Najafi F, Bakhshandeh E, Khonakdar H A, Mostafaiyan M, Simon F, Scheffler C and Mäder E 2015 Highly curable epoxy/MWCNTs nanocomposites: an effective approach to functionalization of carbon nanotubes *Chem. Eng. J.* **259** 117–25
[24] Chen W, Liu P, Liu Y, Wang Q and Duan W 2018 A temperature-induced conductive coating via layer-by-layer assembly of functionalized graphene oxide and carbon nanotubes for a flexible, adjustable response time flame sensor *Chem. Eng. J.* **353** 115–25
[25] Abo-Hamad A, Hayyan M, AlSaadi M A, Mirghani M E S and Hashim M A 2017 Functionalization of carbon nanotubes using eutectic mixtures: A promising route for enhanced aqueous dispersibility and electrochemical activity *Chem. Eng. J.* **311** 326–39
[26] Chen J and Yan L 2017 Recent advances in carbon nanotube-polymer composites *Adv. Mater.* **6** 129–48
[27] Damian C M, Garea S A, Vasile E and Iovu H 2012 Covalent and non-covalent functionalized MWCNTs for improved thermo-mechanical properties of epoxy composites *Composites* B **43** 3507–15
[28] Arrigo R, Bellavia S, Gambarotti C, Dintcheva N T and Carroccio S 2017 Carbon nanotubes-based nanohybrids for multifunctional nanocomposites *J. King Saud Univ. Sci.* **29** 502–9
[29] Zhang A, Luan J, Zheng Y, Sun L and Tang M 2012 Effect of percolation on the electrical conductivity of amino molecules non-covalently coated multi-walled carbon nanotubes/epoxy composites *Appl. Surf. Sci.* **258** 8492–7
[30] Cha J, Jin S, Shim J H, Park C S, Ryu H J and Hong S H 2016 Functionalization of carbon nanotubes for fabrication of CNT/epoxy nanocomposites *Mater. Des.* **95** 1–8
[31] Khare K S, Khabaz F and Khare R 2014 Effect of carbon nanotube functionalization on mechanical and thermal properties of cross-linked epoxy-carbon nanotube nanocomposites: role of strengthening the interfacial interactions *ACS Appl. Mater. Interfaces* **6** 6098–110
[32] Tuncel D 2011 Non-covalent interactions between carbon nanotubes and conjugated polymers *Nanoscale* **3** 3545–54
[33] Dumas L, Bonnaud L, Olivier M, Poorteman M and Dubois P 2013 Facile preparation of a novel high performance benzoxazine-CNT based nano-hybrid network exhibiting outstanding thermo-mechanical properties *Chem. Commun.* **49** 9543–5
[34] Edwards E R, Kostov K G and Botelho E C 2013 Evaluation of the chemical interaction between carbon nanotubes functionalized with TGDDM tetrafunctional resin and hardener DDS *Composites* B **51** 197–203
[35] Liu J Q, Xiao T, Liao K and Wu P 2007 Interfacial design of carbon nanotube polymer composites: a hybrid system of noncovalent and covalent functionalizations *Nanotechnology* **18** 165701
[36] Fujigaya T and Nakashima N 2015 Non-covalent polymer wrapping of carbon nanotubes and the role of wrapped polymers as functional dispersants *Sci. Technol. Adv. Mater.* **16** 024802
[37] Chen Q, Xu R and Yu D 2006 Multiwalled carbon nanotube/polybenzoxazine nanocomposites: preparation, characterization and properties *Polymer* **47** 7711–9
[38] Zúñiga C, Bonnaud L, Lligadas G, Ronda J C, Galià M, Cádiz V and Dubois P 2014 Convenient and solventless preparation of pure carbon nanotube/polybenzoxazine nanocomposites with low percolation threshold and improved thermal and fire properties *J. Mater. Chem.* A **2** 6814–22
[39] Dumas L, Bonnaud L, Olivier M, Poorteman M and Dubois P 2014 High performance benzoxazine/CNT nanohybrid network—an easy and scalable way to combine attractive properties *Eur. Polym. J.* **58** 218–25
[40] Dumas L, Bonnaud L and Dubois P 2016 Novel porous nanohybrid materials with unexpected mechanical and electrical performance by pyrolysis of carbon nanotube-filled benzoxazine thermosets *Nanocomposites* **2** 169–75
[41] Dumas L, Bonnaud L and Dubois P 2017 Polybenzoxazine nanocomposites: case study of carbon nanotubes *Advanced and Emerging Polybenzoxazine Science and Technology* ed H Ishida and P Froimowicz (Amsterdam: Elsevier) pp 767–800
[42] Kaleemullah M, Khan S U and Kim J-K 2012 Effect of surfactant treatment on thermal stability and mechanical properties of CNT/polybenzoxazine nanocomposites *Compos. Sci. Technol.* **72** 1968–76
[43] Liu Y, Wang B and Jing X 2011 Thermal properties of hyperbranched polyborate functionalized multiwall carbon nanotube/polybenzoxazine composites *Polym. Compos.* **32** 1352–61
[44] Wang Y-H, Chang C-M and Liu Y-L 2012 Benzoxazine-functionalized multi-walled carbon nanotubes for preparation of electrically-conductive polybenzoxazines *Polymer* **53** 106–12
[45] Wang C-F, Kuo S-W, Lin C-H, Chen H-G, Liao C-S and Hung P-R 2014 Benzoxazine as a reactive noncovalent dispersant for carbon nanotubes *RSC Adv.* **4** 36012–6

[46] Huang N-J, Zang J, Zhang G-D, Guan L-Z, Li S-N, Zhao L and Tang L-C 2017 Efficient interfacial interaction for improving mechanical properties of polydimethylsiloxane nanocomposites filled with low content of graphene oxide nanoribbons *RSC Adv.* **7** 22045–53
[47] Raimondo M, Guadagno L, Speranza V, Bonnaud L, Dubois P and Lafdi K 2018 Multifunctional graphene/POSS epoxy resin tailored for aircraft lightning strike protection *Composites* B **140** 44–56
[48] Raimondo M, Guadagno L, Vertuccio L, Naddeo C, Barra G, Spinelli G, Lamberti P, Tucci V and Lafdi K 2018 Electrical conductivity of carbon nanofiber reinforced resins: potentiality of tunneling atomic force microscopy (TUNA) technique *Composites* B **143** 148–60
[49] Guadagno L, Raimondo M, Vittoria V, Vertuccio L, Naddeo C, Russo S, De Vivo B, Lamberti P, Spinelli G and Tucci V 2014 Development of epoxy mixtures for application in aeronautics and aerospace *RSC Adv.* **4** 15474–88
[50] Guadagno L *et al* 2015 Correlation between electrical conductivity and manufacturing processes of nanofilled carbon fiber reinforced composites *Composites* B **80** 7–14
[51] Guadagno L *et al* 2015 Effective formulation and processing of nanofilled carbon fiber reinforced composites *RSC Adv.* **5** 6033–42
[52] Guadagno L, Sarno M, Vietri U, Raimondo M, Cirillo C and Ciambelli P 2015 Graphene-based structural adhesive to enhance adhesion performance *RSC Adv.* **5** 27874–86
[53] Baskaran D, Mays J W and Bratcher M S 2005 Noncovalent and nonspecific molecular interactions of polymers with multiwalled carbon nanotubes *Chem. Mater.* **17** 3389–97
[54] Beigbeder A, Linares M, Devalckenaere M, Degée P, Claes M, Beljonne D, Lazzaroni R and Dubois P 2008 CH-p interactions as the driving force for silicone-based nanocomposites with exceptional properties *Adv. Mater.* **20** 1003–7
[55] Al-rubaie L A-r R and Raheem Jameel M 2015 Synthesis, characterization and antibacterial studies of new carboxamide derivatives of dapsone *Iraqi Natl J. Chem.* **15** 41–58
[56] Jiang L, Huang Y, Zhang Q, He H, Xu Y and Mei X 2014 Preparation and solid-state characterization of dapsone drug–drug co-crystals *Cryst. Growth Des.* **14** 4562–73
[57] Thirukumaran P, Sathiyamoorthi R, Shakila Parveen A and Sarojadev M 2016 New benzoxazines from renewable resources for green composite applications *Polym. Compos.* **37** 573–82
[58] Johnson L M, Gao L, Shields C W IV, Smith M, Efimenko K, Cushing K, Genzer J and López G P 2013 Elastomeric microparticles for acoustic mediated bioseparations *J. Nanobiotechnol.* **11** 22
[59] Zhao Z, Dai Y, Ge G and Wang G 2015 Efficient tuning of microstructure and surface chemistry of nanocarbon catalysts for ethylbenzene direct dehydrogenation *AIChE J.* **61** 2543–61
[60] Le V T, Ngo C L, Le Q T, Ngo T T, Nguyen D N and Vu M T 2013 *Adv. Nat. Sci.: Nanosci. Nanotechnol.* **4** 035017
[61] Murphy H, Papakonstantinou P and Okpalug T I T 2006 Raman study of multiwalled carbon nanotubes functionalized with oxygen groups *J. Vac. Sci. Technol.* B **24** 715–20
[62] Fantini C, Pimenta M A and Strano M S 2008 Two-phonon combination raman modes in covalently functionalized single-wall carbon nanotubes *J. Phys. Chem.* C **112** 13150–5
[63] Jung W R, Choi J H, Lee N, Shin K, Moon J-H and Seo Y-S 2012 Reduced damage to carbon nanotubes during ultrasound-assisted dispersion as a result of supercritical-fluid treatment *Carbon* **50** 633–6
[64] Osorio A G, Silveira I C L, Bueno V L and Bergmann C P 2008 H_2SO_4/HNO_3/HCl functionalization and its effect on dispersion of carbon nanotubes in aqueous media *Appl. Surf. Sci.* **255** 2485–9
[65] Castro V G, Costa I B, Lopes M C, Lavall R L, Figueiredo K C S, Silva G G and Braz J 2017 Tailored degree of functionalization and length preservation of multiwalled carbon nanotubes by an optimized acid treatment process *Chem. Soc.* **28** 1158–66
[66] Dresselhaus M S, Jorio A, Souza Filho A G and Saito R 2010 Defect characterization in graphene and carbon nanotubes using Raman spectroscopy *Phil. Trans. R. Soc.* A **368** 5355–77
[67] Golosova A A, Papadakis C M and Jordan R 2011 Chemical functionalization of carbon nanotubes with aryl diazonium salts *MRS Proc.* **1362** 1–6
[68] Guadagno L, De Vivo B, Di Bartolomeo A, Lamberti P, Sorrentino A, Tucci V, Vertuccio L and Vittoria V 2011 Effect of functionalization on the thermo-mechanicaland electrical behavior of multi-wall carbon nanotube/epoxycomposites *Carbon* **49** 1919–30
[69] Cha J, Jin S, Shim J H, Park C S, Ryu H J and Hong S H 2016 Functionalization of carbon nanotubes for fabrication of CNT/epoxy nanocomposites *Mater. Des.* **95** 1–8
[70] Maultzsch J, Reich S and Thomsen C 2002 Raman characterization of boron-doped multiwalled carbon nanotubes *Appl. Phys. Lett.* **81** 2647–9
[71] Hou C, Tai Z, Zhao L, Zhai Y, Hou Y, Fan Y, Dang F, Wang J and Liu H 2018 High performance MnO@C microcages with a hierarchical structure and tunable carbon shell for efficient and durable lithium storage *J. Mater. Chem.* A **6** 9723–36
[72] Hergeth W-D, Steinau U-J, Bittrich H-J, Simon G and Schmutzler K 1989 Polymerization in the presence of seeds: IV. Emulsion polymers containing inorganic filler particles *Polymer* **30** 254–8
[73] Kotsilkova R, Fragiadakis D and Pissis P 2005 Reinforcement effect of carbon nanofillers in an epoxy resin system: Rheology, molecular dynamics, and mechanical studies *J. Polym. Sci.* B **43** 522–33
[74] Sun Y, Zhang Z, Moon K-S and Wong C P 2004 Glass transition and relaxation behavior of epoxy nanocomposites *J. Polym. Sci.* B **42** 3849–58
[75] Li B and Zhong W-H 2011 Review on polymer/graphite nanoplatelet nanocomposites *J. Mater. Sci.* **46** 5595–614
[76] Zhou T, Wang X, Liu X and Xiong D 2009 Influence of multi-walled carbon nanotubes on the cure behavior of epoxy-imidazole system *Carbon* **47** 1112–8